The added value of IMERG in characterizing rainfall in tropical cyclones

Manuel F. Rios Gaona[a,*], Gabriele Villarini[a], Wei Zhang[a], Gabriel A. Vecchi[b,c]

[a] *IIHR - Hydroscience & Engineering, The University of Iowa, Iowa City, Iowa, USA.*

[b] *Department of Geosciences, Princeton University, Princeton, New Jersey, USA.*

[c] *Princeton Environmental Institute, Princeton University, Princeton, New Jersey, USA.*

Abstract

Heavy rainfall associated with landfalling tropical cyclones (TCs) is responsible for significant societal and economic impacts. Improved characterization and description of how rainfall during these storms changes as a function of distance from the center of circulation are critical to increase our preparedness against this natural hazard. Since March 2014, the hydrometeorological community has benefitted from the Global Precipitation Measurement mission (GPM), especially with its gridded-rainfall product IMERG (Integrated Multi-satellitE Retrievals for GPM), which offers global rainfall estimates with a spatiotemporal resolution of $0.1^\circ \times 0.1^\circ$ every 30 minutes, on a near-real time basis.

We analyze here 166 TCs worldwide from March 2014 through March 2016. For every TC, we extract from IMERG V04 a 2,000 km rainfall swath along the TC track. This allows us to characterize with great accuracy the spatial structure of TC-rainfall, from its development all the way to its landfall and dissipation. We stratify the analyses by basin of origin, intensity of the storm, and whether the TC was over ocean or land. We find that the South Pacific, West Pacific, and North Indian basins yield (median) rainfall intensities between 6 and 7.5 $mm \cdot h^{-1}$ at radii $\sim$50 km. These intensities are for TCs over ocean, and in most

*Corresponding author

Email address: manuelfelipe-riosgaona@uiowa.edu (Manuel F. Rios Gaona)

cases they are twice (or more) as high as the median intensities for TCs over land ($\sim$3.0 mm$\cdot$h^{-1}). For the North Atlantic, South Indian, and East Pacific basins the oceanic (median) rainfall intensities are between 4 and 5 mm$\cdot$h^{-1}. Upscaled IMERG estimates ($0.25^\circ \times 0.25^\circ$ every 3 hours) do not capture the rainfall structure within the eyewall (i.e., for radii < 50 km), especially for the South Pacific, West Pacific, and North Indian basins.

Keywords: Tropical Cyclones, IMERG, Rainfall

---

1. Introduction

Very often tropical cyclones (TCs) have catastrophic impacts on society due to the vast amount of rainfall they carry. Coastal areas are the most prone regions to such devastating impacts. Still, heavy rainfall from TCs often reaches areas located hundreds of kilometers inland (e.g., Czajkowski et al., 2017; Khouakhi et al., 2017). For instance, the two most devastating TCs in 2016, i.e., Hurricane Matthew (September 28 to October 10, affecting Haiti, Cuba, the Bahamas, and the U.S. West Coast - North Atlantic basin), and Typhoon Lionrock (August 29 to September 1, affecting North Korea, east China, and Japan - West Pacific basin) accounted for $\sim$14% of human fatalities caused by natural disasters in 2016 (1,155 deaths; Impact Forecasting, 2017). With 92 USD billions, TCs and flooding accounted for the $\sim$44% of global economic losses by natural disasters in 2016 (Impact Forecasting, 2017).

In the United States (U.S.), floods associated with TCs claim a large toll in terms of fatalities (Rappaport, 2014, 2000; Elsberry, 2002). Czajkowski et al. (2017) established a methodology to relate intensity of TC flood events and economic losses, under current and future conditions. They found that in coastal areas 45% of the floods in the U.S. come from landfalling TCs (55% for inland areas). This is worrisome not just for the U.S. but also globally because the continuous growth of (coastal) population increases the risk associated with TCs and flooding (Rappaport, 2000).

Improved modeling and characterization of the precipitation associated with TCs provide basic information to increase our preparedness against this hazard. Furthermore, the development of parametric models of rainfall distribution from TCs is useful in a number of fields, such as operational forecasting and warning, climatological risk assessment, and engineering design (Kepert, 2010). While parametric models that describe the wind speed around the center of circulation of the storm have been developed (e.g., Holland, 2008), parametric models that characterize TC-rainfall still lag behind (e.g., Lonfat et al., 2007). However, there have been efforts towards the characterization of rainfall associated with these storms, given the high resolution of satellite-based rainfall estimates (Prat & Nelson, 2016; Jiang et al., 2008b; Lonfat et al., 2004). Prat & Nelson (2016) analyze 12 years of satellite data to estimate the contribution of TCs to extreme daily rainfall. Lonfat et al. (2004) provide global characterizations of TC-rainfall through satellite measurements, which represent a step forward to understand and improve current techniques in quantitative precipitation forecasting (QPF) of TCs, and to reduce uncertainties in QPF due to the lack of precipitation data over the oceans (see also Jiang et al., 2008a). The evaluation and validation of numerical weather prediction models rely on oceanic precipitation data, which is often based on a very limited number of ground-based sensors (e.g., rain gauges, radars). As pointed out by Tuleya et al. (2007), one major issue in accurately forecasting TC-rainfall is tied to the small scale at which heavy precipitation manifests itself (see also Luitel et al., 2016). Hence, the main advantage of high-resolution satellite rainfall products is their ability to track these large storms, for which accurate rainfall estimates are difficult to obtain from ground-based sensors. This is even more difficult near the storm center where the rain rates are the highest (Lonfat et al., 2007; Elsberry, 2002).

IMERG (Integrated Multi-satellitE Retrievals for GPM - Global Precipitation Measurement mission) is a high-resolution satellite product that has the potential to improve the characterization of rainfall associated with TCs. It is a gridded rainfall product with a spatiotemporal resolution of $0.1^\circ \times 0.1^\circ$ every

30 minutes between 60°N-60°S (Hou et al., 2014). Khouakhi et al. (2017) preferred rain gauges over satellite estimates for TC-rainfall characterization, given that satellite-rainfall estimates often represent short historical records, relatively coarse resolution, and are affected by large uncertainties. Issues associated with the relatively coarse spatiotemporal resolution of satellite rainfall products and their uncertainties have been improved with the recent upgrade in IMERG V04 (Huffman et al., 2017c). IMERG is available since March 2014, and although it is still a product in development, its high spatiotemporal resolution holds promises on critical aspects towards improved QPF of TCs. Elsberry (2002) refers to such critical aspects as track predictability, rainfall distribution, rainfall duration, rainfall totals (even over smaller regions), and a better resolved precipitation gradient. GMI (GPM Microwave Imager) is the most advanced conical-scanning passive microwave radiometer. With 13 channels (10.65 to 183.31±7 GHz) it detects a wide range of precipitation intensities, from heavy to light precipitation (Rios Gaona et al., 2016; Hou et al., 2014). Thus, GPM rainfall products now provide better-resolved precipitation gradients.

We analyze here 166 TCs that occurred worldwide in a 2-year period. The analysis is stratified by basin of origin, storm category, and whether the storm is over the ocean or land. To highlight the impacts of coarser-resolution products on the characterization of TC-rainfall, we resample the IMERG product to a 3-hour $0.25^\circ \times 0.25^\circ$ resolution. Luitel et al. (2016) and Villarini et al. (2011) analyzed high-resolution rainfall products such as Stage IV primarily for the conterminous US. Similarly, Jiang et al. (2008a) analyzed 6 years of TRMM (Tropical Rainfall Measuring Mission) 3B42 (3-hourly, $0.25^\circ \times 0.25^\circ$ resolution) estimates to characterize TC rainfall in the NA basin, namely U.S., and studied the relation between the rainfall potential (before landfall) and the maximum storm total rainfall for landfalling TCs. Their analysis was also stratified by land/ocean and by storm intensity. High-resolution rainfall products such as IMERG make it possible to perform more comprehensive analyses given the vast amount data they offer over the oceans. Our work is one of the first studies

to analyze the precipitation characteristics within TCs at high spatiotemporal resolutions on a global scale. We provide an in-depth and global characterization of rainfall distribution from TCs, which can be useful towards the development of further improved TC parametric models.

This paper is organized as follows: Sections 2 and 3 describe the two data sets involved in this study, and the methodology to merge them both, respectively. The results and discussion of our major findings are presented alongside in Section 4. Conclusions and recommendations are provided in Section 5.

2. Data

For the period of March 2014 through March 2016, we analyze and merge two data sets: IBTrACS, and IMERG V04 Final.

The IBTrACS (International Best Track Archive for Climate Stewardship) is a comprehensive worldwide collection of TC best-track data, from all the Regional Specialized Meteorological Centers (RSMCs) and Tropical Cyclone Warning Centres (TCWCs) within the World Meteorological Organization (WMO), and other national agencies (Knapp et al., 2010) (IBTrACS data is freely available from the server `ftp://eclipse.ncdc.noaa.gov/pub/ibtracs/`). IBTrACS was developed by the National Climatic Data Center (NCDC) jointly with the World Data Center for Meteorology. It contains 27 storm attributes for seven global basins: North Atlantic (NA), Eastern Pacific (EP), Western Pacific (WP), Northern Indian Ocean (NI), Southern Indian Ocean (SI), South Pacific (SP), and South Atlantic (SA) (Fig. 1). From these attributes we use longitude and latitude of the storm centers (to interpolate the TC track at 30-minute resolution), maximum sustained wind speed (MSW, to categorize the storm according to the Saffir-Simpson Hurricane Scale - SSHS; Simpson, 1974), the basin of origin, and the time at landfall (if existent). The temporal resolution of this data set is 6 hourly (00:00, 06:00, 12:00, and 18:00 UTC). We analyze 166 TCs in total, of which 65 occurred in 2014, 96 in 2015, and 5 since January until March

2016. There were 91 TCs in total for 2014 but we only consider 65 given the availability of IMERG V04 Final. For any given year, IBTrACS posts the post-season reanalysis (of that given year) in the last quarter of the next year. There were thus only five TCs for 2016. Figure 1 shows the tracks of the 166 TCs we focused on. This figure also shows the seven global basins in which the Earths surface is divided.

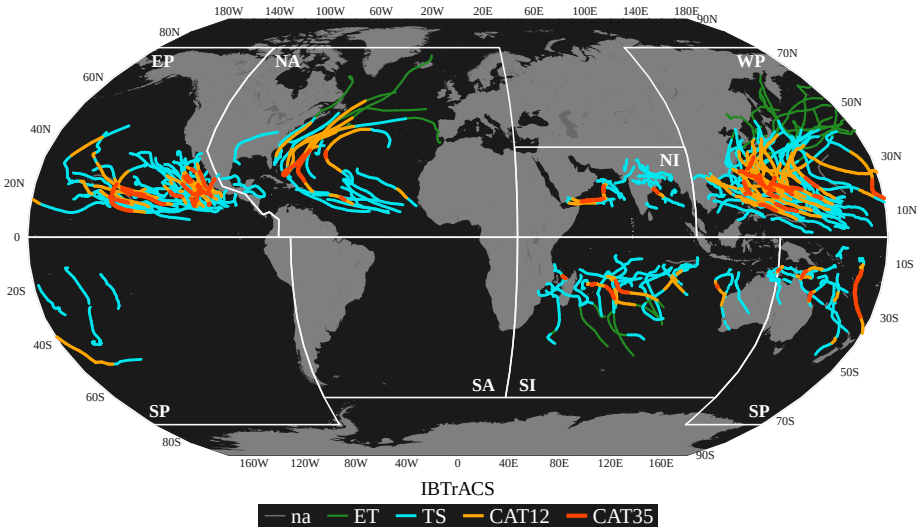

Figure 1: Spatial distribution of 166 TCs (IBTrACS) from March 2014 through March 2016. The color scale represents the TC intensities: green for ET (Extra-Tropical), cyan for TS (MSW $<$ 64 kt; 33.1 m$\cdot$s^{-1}), light orange for CAT12 (64 $\leqslant$ MSW $<$ 96 kt; 33.1 - 49.4 m$\cdot$s^{-1}), and dark orange for CAT35 (MSW $\geqslant$ 96 kt). Light grey tracks (na) are those IBTrACS in 2016 for which no IMERG data is available. The white divisions show the seven basins according to Knapp et al. (2010), i.e., East Pacific (EP), North Atlantic (NA), North Indian (NI), West Pacific (WP), South Pacific (SP), South Atlantic (SA), and South Indian (SI).

IMERG V04 Final contain several subsets, from which the *precipitationCal* subset offers the most accurate rainfall estimates. It is a gridded rainfall product (level 3) from the GPM mission (GPM rainfall datasets are freely available at the National Aeronautics and Space Administration - NASA - website `http://pmm.nasa.gov/data-access/downloads/gpm`). It provides rainfall intensities with a spatiotemporal resolution of 0.1°$\times$0.1° every 30 minutes. This

product is obtained by processing (i.e., intercalibration, merging, and spatiotemporal interpolation) all the microwave precipitation estimates available from the GPM constellation (Huffman et al., 2017a). IMERG also incorporates infrared data from geostationary satellites, and it is calibrated with global gauge analyses of precipitation (Schneider et al., 2015a,b). Huffman et al. (2017a,b,c) offer a detailed and very technical information on the recent update of IMERG V04 (Final). The availability of this data set goes from March 12, 2014 to the present with a latency of 4 months. Hence, the number of analyzed TCs is limited to the availability of this data set. From here onwards, IMERG V04 Final (*precipitationCal* subset) will be referred only as IMERG.

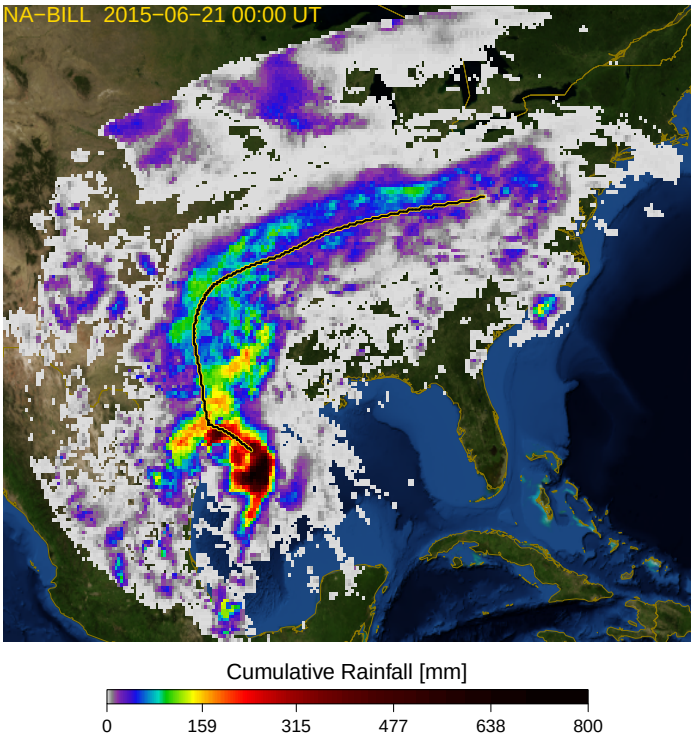

Figure 2: Total rainfall for the Tropical Storm Bill (16 June 2016 at 00:00 UTC through 21 June 2016 at 00:00 UTC). The figure shows cumulative rainfall for a 1,000-km radius along the TC track (yellow-black line). The relief is downloaded from `https://earthobservatory.nasa.gov/Features/BlueMarble/` (Stöckli et al., 2006).

3. Methodology

We downscaled IBTrACS attributes from their native 6-hour temporal resolution to 30-minute IMERG native resolution. We interpolated the 6-hour latitudes and longitudes via spline cubic interpolation to estimate the TC center at 30-minute intervals. We then extracted the 30-minute rainfall intensities from the IMERG data set over a radius of 1,000 km. These 30-minute rainfall fields were aggregated throughout the storms lifetime (see Fig. 2 for one example; the supplemental material shows the GIF movie for the whole duration of TC Bill).

Profiles of rainfall intensity as a function of distance from the TC center were extracted for every 30-minute interpolated center. We computed the average rainfall intensity for radii every 7 km from the TC center outwards (i.e., 0 km, 7 km, 14 km ...) to ensure a regular sampling of IMERG gridded-rainfall given its spatial resolution (i.e., $0.1^\circ \times 0.1^\circ$ or $\sim 11 \times 11$ km^2 at equatorial latitudes). Once we obtained these averaged profiles, we stratified them into three categories: 1) basin of origin, 2) TC intensity, and 3) land or ocean. We based this categorization on the coordinates of the TC center and the MSW stored in the IBTrACS. A TC is overland if the center of the storm has crossed the coastline. The MSW for a given 30-minute TC center corresponded to the previous 6-hourly step stored in the IBTrACS. Given the coordinates of the TC centers, we established whether the TC center was located over ocean or land. We re-categorized the TC intensity into four categories based on the SSHS: for MSW $<$ 64 kt (33.1 m$\cdot$s^{-1}, TS), for 64 $\leqslant$ MSW $<$ 96 kt (33.1 - 49.4 m$\cdot$s^{-1}, CAT12), for MSW $\geqslant$ 96 kt (CAT35), and extra-tropical cyclones (ET).

For the upscaled 3-hourly rainfall fields, we computed rainfall intensity profiles for radii every 33 km (i.e., 0 km, 33 km, 66km ...) to also ensure a regular sampling of IMERG upscaled- and gridded-rainfall (i.e., $0.25^\circ \times 0.25^\circ$ or $\sim 28 \times 28$ km^2 at equatorial latitudes). This spatiotemporal resolution is consistent with other high-resolution satellite products such as TMPA (TRMM Multisatellite Precipitation Analysis; Huffman et al., 2007), and CMORPH (the Climate Pre-

diction Center morphing method; Joyce et al., 2004). We also applied the same
162 analysis steps (i.e., by basin of origin, TC intensity, and land or ocean) to the upscaled 3-hourly rainfall fields.

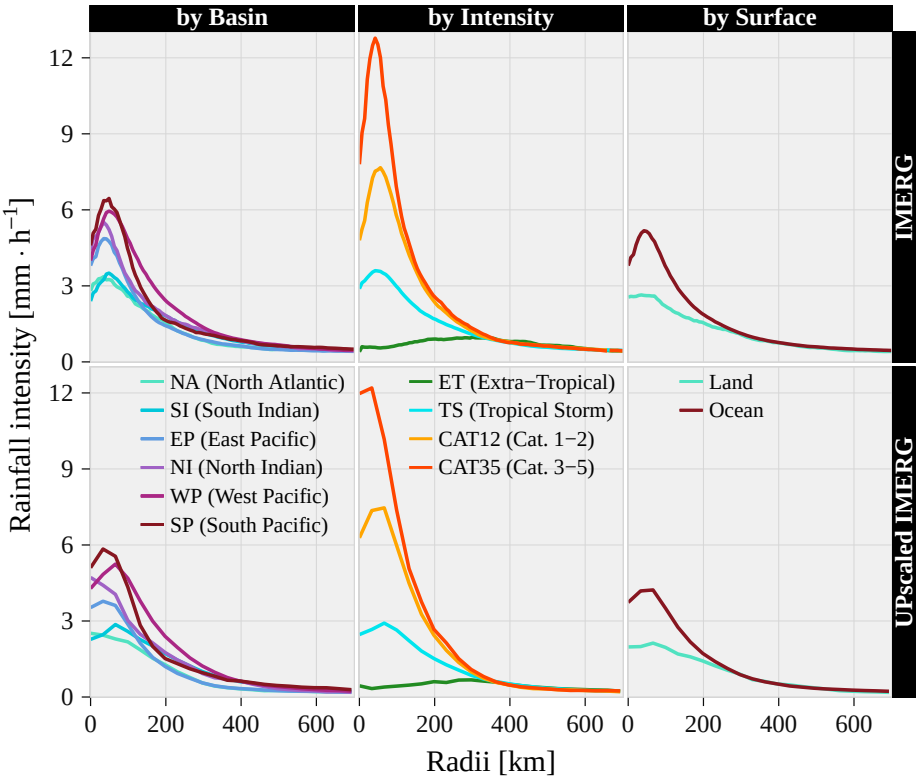

Figure 3: Spatial structure of TC rainfall for 166 TCs from March 2014 through March 2016. The profiles indicate the 50^{th} percentile by basin of origin (left column), by intensity (middle column), and whether the storm center was over land or ocean (right column). The spatiotemporal resolution of the top row (IMERG) is $0.1° \times 0.1°$ every 30 minutes, whereas for the bottom row (Upscaled IMERG) is $0.25° \times 0.25°$ every 3 hours.

164 4. Results and Discussion

The Pacific basin is the one where most of the TCs develop (North Pacific), and
166 the one with the most intense TCs (South Pacific). Figures 3 and 4 show the general overview of the three main analyses we focused on. For instance, the

West and East Pacific basins (WP and EP, respectively) account for 61.8% of all the analyzed data. We analyzed ∼4.8 million radii of average rainfall intensities from IMERG (at its native resolution) for all 166 TCs. Out of the 61.8%, 31.1% corresponds to TCs from CAT12 and CAT35 intensities (Fig. 3 - middle column, and Fig. 4). Tropical storms (TS) account for 68.4% of the storms across all six basins studied here (Fig. 4), with an average rainfall intensity of ∼4 mm·h^{-1} close to the eyewall (Fig. 3). CAT12 bring twice as much rainfall as TSs do, whereas CAT35 TCs bring three times more rainfall than TSs do (13 mm·h^{-1}, Fig. 3 - middle column). Even though the orientation and size of TCs can affect coastal communities even if they do not make landfall, their destructive power is largely perceived and quantified after landfalling.

Rainfall from landfalling storms amounts to 7% of the overall analyzed rainfall (∼4.8×10^6 counts; Fig. 4). The NI basin was the least affected by TCs in the studied period (5.3%; Fig. 4). Nevertheless, it is the basin with the largest proportion of landfalling TCs with 39.7% of all TCs for that basin (about one third of all landfalling TCs combined). Average rainfall intensity over oceans is almost twice as large as the rainfall intensity over land (Fig. 3 - right panels). The rainfall structure over the ocean clearly indicates the peak intensity close to the eyewall, whereas for landfalling TCs such a peak is not nearly as marked. As suggested by Tuleya et al. (2007), the decrease of rainfall rate as the TCs breaks inland is related to the decrease of the primary circulation of the storm.

Figure 3 (bottom row) shows the deficiency of upscaled data sets to reproduce extreme values, conversely to the case with high-resolution data sets (Tustison et al., 2001). Upscaled or coarser data sets do not reproduce either extreme (or peak) values or the rise to the peak within the eyewall, clearly captured by the high-resolution IMERG data set (Fig. 3 - top row). Thus, this proves the potential capabilities of such a data set to model TC rainfall with more accuracy and a much higher level of detail. Figure 3 (bottom row) is based on ∼255,000 radii of average rainfall intensities from the upscaled IMERG data set (∼5% of the native IMERG data set). The distribution of this upscaled

198 data set (not shown here) is almost identical to that in Fig. 4. The radial distribution (structure) of landfalling TCs in Fig. 3 is consistent with similar
200 results previously presented by Lonfat et al. (2007, 2004), Marchok et al. (2007), and Tuleya et al. (2007).

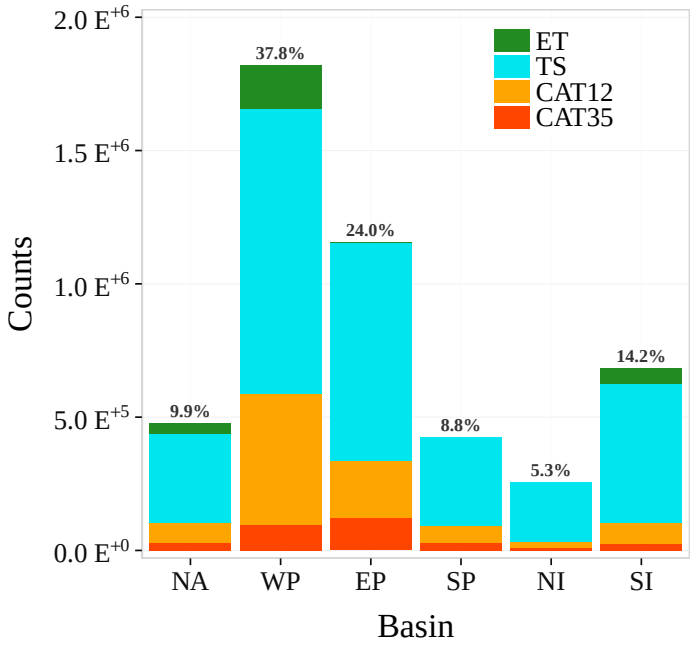

Figure 4: TC distribution for $\sim 4.8 \times 10^6$ radii of average rainfall intensities (for 166 TCs from March 2014 through March 2016). Each bar represents the percentage of TCs that originated within that basin. The colors in each bar indicate the proportion of TCs with regard to the intensity of the storm. See Supplementary Fig. 1 for the proportions of TCs with regard to the surface stratification.

202 Figure 5 shows a detailed multi-analysis of the IMERG data set by basin, intensity, and ocean/land. The data is first stratified by basin of origin, with the
204 development of TCs mostly in the East and West Pacific basins, and in minor proportion in the South Indian and North Atlantic basins (i.e., higher number
206 of counts indicated by the green color). On average, high-intensity TCs develop in the West and South Pacific, and NI basins. This is demonstrated by the
208 black curve, which summarizes the rainfall profiles regardless of the TC intensity. Furthermore, the proportion of TCs is larger over ocean than land (see also

Supplementary Fig. 1), as there are more counts for ocean-based storm centers (97%) than for land-based ones (3%). TCs are still associated with heavy rainfall over land, even though they become weaker as they move inland, and are generally stronger over the ocean and at landfall. This is because TCs generate heavy rainfall by interacting with topography while with much less moisture supply from the ocean to sustain the intensity after landfall (Emanuel, 2005; Bender et al., 1985). The only case in which there is no practical difference between ocean or land is in the South Indian basin, where the median maximum (rainfall) intensity is about $\sim$3 mm$\cdot$h^{-1} for radii $\sim$50 km (eyewall).

The high-resolution IMERG data set allows a clear characterization of TC-rainfall over ocean or land. When the storm is over the ocean, rainfall intensities increase from the center of circulation to $\sim$50 km outwards. This reflects a clear definition of the storms eye and eyewall (the heavy rainfall band just beyond the eye of the storm). The evolution (e.g., breakdown) of eyewall in TCs are closely associated with intensity change after landfall (Wang & Wu, 2004; Wu et al., 2003). If we focus on all the landfalling storms, and on those that underwent extratropical transition, we do not clearly see this well-defined structure due to the collapse of the eyewall and the formation of outer rainbands (Figure 5). Even though land-based satellite retrievals are in general more accurate than ocean-based ones due to gauge adjustment (Huffman et al., 2017a), improvements on IMERG Final V04 (Huffman et al., 2017c) drastically reduce discrepancies and uncertainties in the transition between ocean and land rainfall retrievals. The average rainfall rate and total rain of landfalling TCs are profoundly influenced by the intensity of TCs associated with TC circulation and the horizontal distribution of convection during landfall (Yu et al., 2017; Alvey III et al., 2015).

On average, the SP, WP, and NI basins are the ones with the higher (median) rainfall intensities, between 6 and 7.5 mm$\cdot$h^{-1} at radii $\sim$50 km. Such intensities refer to estimates over ocean, and in most cases they are twice (or more) as high as the median intensities for inland structures, i.e., $\sim$3.0 mm$\cdot$h^{-1} (Fig. 5

- black profiles). The distribution of rainfall intensities in such basins (i.e., SP, WP, and NI) may be related to a higher mean sea surface temperature (SST) in these basins when compared to other basins because a higher SST tends to lead to saturation water vapour specific humidity (e.g., Lin et al., 2015; Langousis & Veneziano, 2009). The NA, SI, and EP basins do not show as high TC-rainfall as the other three basins, i.e., between 4 and 5 mm·h^{-1}. In all these cases, the peak of the median rainfall intensity generally occurs at radii ∼50 km. Our results for the NA basin are in line with Jiang et al. (2008a). They found that the maximum mean rain rate over ocean was ∼5.0 mm·h^{-1} (within 50 km of the TC center), whereas over land it was ∼1.6 mm·h^{-1} (Fig. 5 - "NA (North Atlantic), Land" panel).

In general, TC rainfall is more intense over the ocean than over land (Fig. 3 - by Surface), with the pattern of high median rainfall over ocean (Fig. 5 - black profiles) mainly governed by the behaviour of the TS category, given that the majority of TCs fall under this category (Fig. 4, and Sec. 4). There are few cases in which TC-rainfall is higher over the land than over the ocean, especially for the CAT12 and CAT35. We see such a behaviour, for instance, in the three basins with the highest median TC-rainfall (Fig. 5 - SP, WP, and NI). Nevertheless, we remind the reader that these are very few cases as indicated by the scatter density plots (e.g., CAT35 profile in Fig. 5 - WP, Ocean is computed from ∼5,000 counts; whereas CAT35 profile in Fig. 5 - WP, Land is computed from ∼10 counts). Conversely to TS, CAT12 and CAT35 show a devastating power after landfall, as these two latter categories are the ones with the more intense rainfall intensities and wind speeds. From Fig. 5 one can also see that the proportion of CAT12 and CAT35 events (26.2%) is much smaller than TS events (68.4%). Figure 4 presents similar results. Prat & Nelson (2013) studied the contribution of TC rainfall to global rainfall via the TMPA 3B42 product. For a 12-year period they found that the WP basin (East Asia for them) was the one with the highest TC rainfall over land ($>$ 360 mm·year^{-1}), despite its lower cyclonic activity against the NA basin (i.e., 30%. less).

Our results are also consistent with those obtained by Lonfat et al. (2004), in which the NI and WP basins show the largest mean rain rates ($\sim$6.5 mm$\cdot$h^{-1}), and in which the mean rain rates for the NA and EP (over land) are quite similar to those obtained here ($\sim$5 mm$\cdot$h^{-1}) (Fig. 5 - "..., Land" panels). Lonfat et al. (2004) based their analyses on 260 TCs worldwide (1998-2000) estimated from TMI data (TRMM Microwave Imager). They also stratified their analyses by basin and storm intensity. Nevertheless, they did not consider land observations as they argued that the TMI rain algorithm underestimated light rain over land. In our case, the IMERG algorithm compensates for such biases (Huffman et al., 2017c). Conversely to our case, Lonfat et al. (2004) acknowledged their lack of significance in their results with regard to CAT12 and CAT35 intensities, given the spatiotemporal resolution of their data set.

So far, we have focused on the IMERG data at its native resolution; nevertheless, we also examined what the results would be once we coarsen its spatiotemporal resolution. Figure 6 shows how the decrease in spatiotemporal resolution results in a loss of detail in the rainfall structure within the eyewall. The high-resolution IMERG data set adds on the representativeness of the results as it is $\sim$20 times larger than the upscaled IMERG data set. Still, the most significant drawback from low-resolution rainfall estimates is their inability to capture the rainfall structure within the eyewall (i.e., for radii $<$ 50 km). This is especially the case for CAT12 and CAT35 intensities, and for the SP, NI, and WP basins (see also Fig. 3). An accurate characterization of TC-rainfall for CAT12 and CAT35 events is extremely important as these type of storms are the ones which brought the most havoc. When compared to Fig. 5, the upscaled structure from CAT12 and CAT35 intensities does not capture the rise to the peak ($\sim$50 km; Fig. 6 - light and dark orange lines, respectively), otherwise well captured by the IMERG data. Hence, high-resolution fields (e.g. rainfall) have higher variability than low-resolution averaged fields, which by nature cannot reproduce the extreme values and high frequency that high-resolution does (Marchok et al., 2007; Tustison et al., 2001).

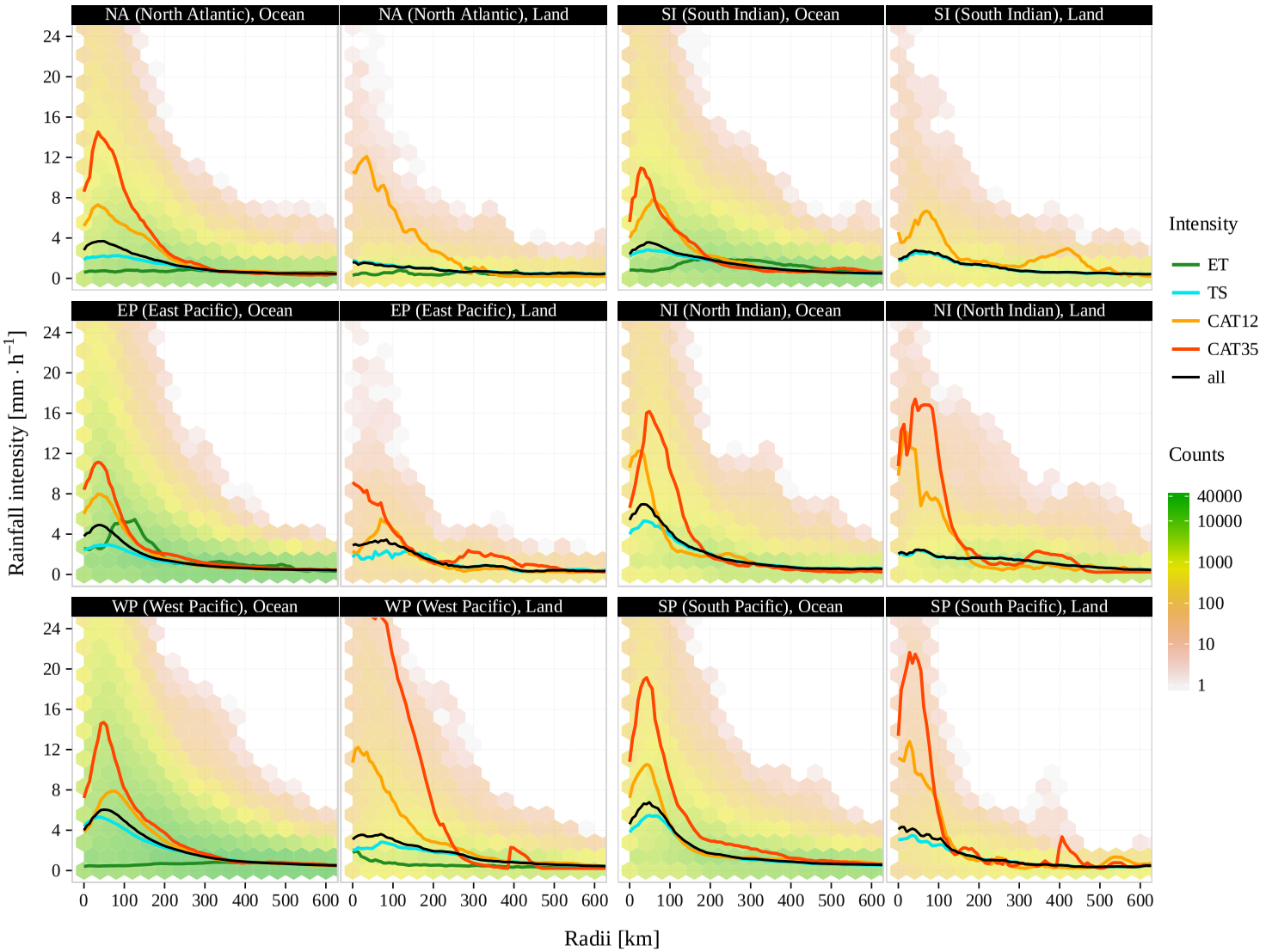

Figure 5: Scatter density plots of mean rainfall intensity against distance from TC center for IMERG rainfall estimates (0.1°×0.1° every 30 minutes). The color scale is logarithmic, and indicates the counts per hexagonal bin. The curves represent rainfall intensity profiles for four intensity levels, and the black curve represents the analyses regardless of the intensity of the event. The plot is divided into six basins of origin, and these are further stratified by ocean and land.

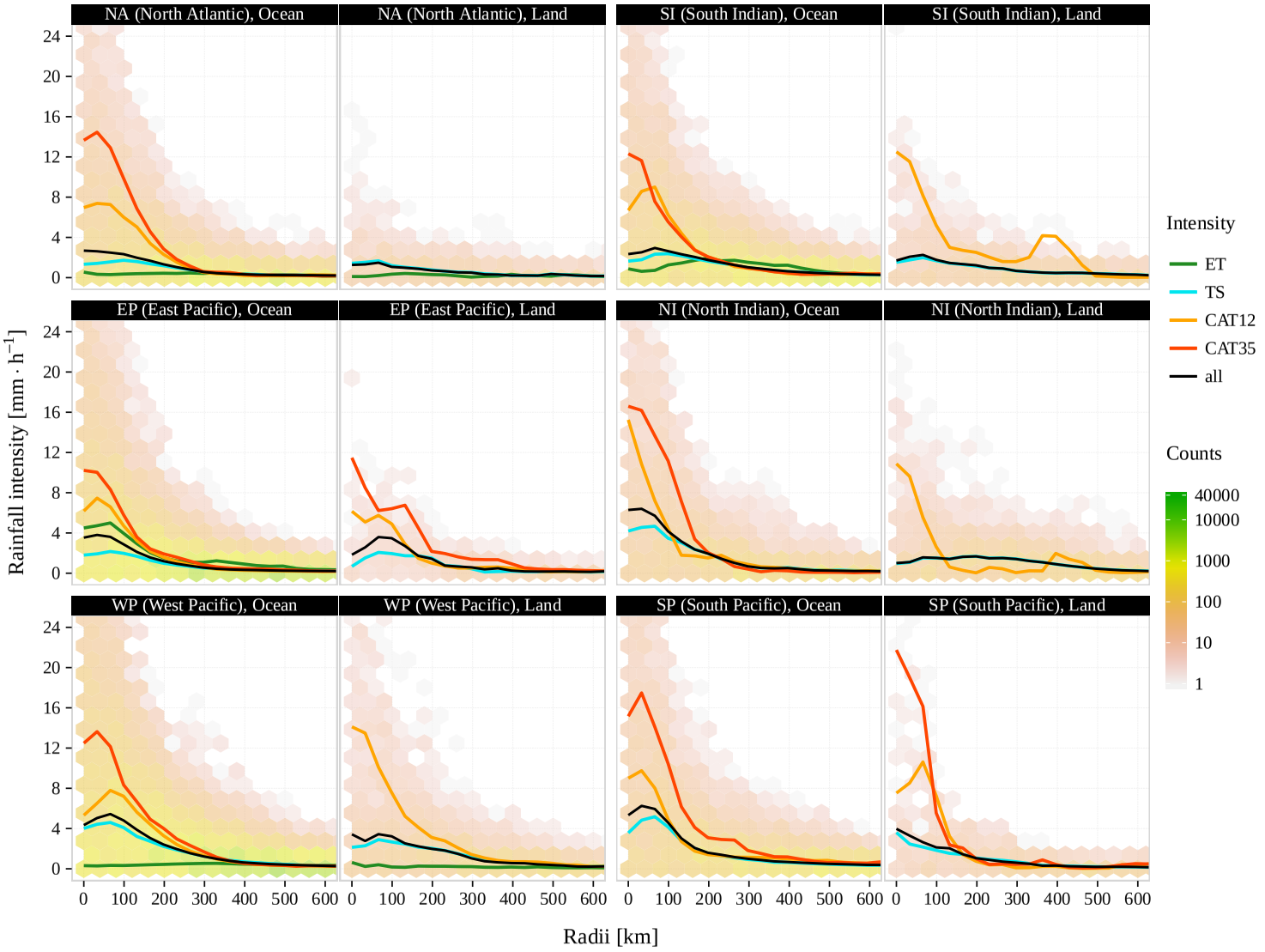

Figure 6: Same as Figure 5 but for the lower resolution (i.e., 0.25°×0.25° every 3 hours).

Coarser TC-rainfall estimates miss not only the rainfall structure within the eyewall but also relevant TCs. Some CAT12 and CAT35 events are missing, and there is a much higher contribution from TS. This is why in Fig. 6 the light orange line (CAT12 - "..., Land" panel, NA basin), and the dark orange lines (CAT35 - "..., Land" panels, WP and NI basins) do not appear in this figure, whereas they do appear in Fig. 5. In fact, the upscaled IMERG data set completely misses the most intense event(s) for the studied period (Figs 5 and 6 - WP basin, "..., Land" panel). Because we stratify a TC as "land" if its IMERG-pixel center was classified as "land", it is more likely for 30-minute (than for 3-hourly) TC centers to be interpolated over land surfaces. Hence, high-resolution rainfall estimates from satellite, namely IMERG, offer a clear opportunity to advance TC-rainfall modeling.

5. Summary and Conclusions

We analyzed 166 TCs from the IBTrACS data set, which represents a thorough global collection of TC best-track data. Our main motivation was to test the performance of high-resolution rainfall estimates from the updated IMERG (V04) product, which is the research product from the GPM mission. IMERG is a gridded satellite product, which offers rainfall estimates between 60°N-60°S at a spatiotemporal resolution of $0.1^\circ \times 0.1^\circ$ every 30 minutes, with a latency of 4 months, starting from March 2014. When both data sets were cross-referenced, we extracted rainfall fields for a 2,000 km-wide swath along the path of each of the 166 TCs. The period of analysis was from March 2014 through March 2016. We split our analysis by basin of origin, storm intensity, and whether the TC center was over the ocean or land. The evaluation was done through rain intensity profiles, and it was repeated for a coarsened resolution of IMERG to show the benefits of high-resolution estimates in TC-rainfall modeling.

Given its high spatiotemporal resolution, we found that IMERG captures quite in detail the spatial structure of rainfall associated with these storms, especially

within the first 100 km from the TC center outwards. We showed, for instance, how it is possible for this high-resolution data set to capture the rise of the rain peak (storm eyewall) for radii < 50 km. This was not the case for the upscaled IMERG data set, which also missed the most intense event(s) of the entire analyzed period.

The WP and EP basins accounted for 61.8% of all TCs, with about one third of these storms belonging to the CAT12 and CAT35 categories. When we stratified the analyses by land/ocean, we found that only 7% of the TCs correspond to landfalling TCs. Yet, we remind ourselves that it is within this 7% that most of the human catastrophes related to flooding from TC-rainfall take place. The NI basin is the least struck by TCs (5.3%), and yet it is the basin with the largest proportion of landfalling TCs (39.7%), which is about one third of all landfalling TCs.

Apart from the different TC-structures among basins, and their related intensities, IMERG allowed us to identify the distinctive TC-structure between ocean and inland. We found that the average rain rate over oceans is almost twice as large as the one inland. Over the oceans, TC-rainfall clearly develops a peak intensity in the eyewall, whereas for landfalling TCs such a peak does not exist (see for instance, Tuleya et al., 2007).

Our approach classifies as land those TCs for which their storm centers are located inland. Another approach would be that of Jiang et al. (2008a,b) in which at least 60% of the rainfall pixels should be over ocean to consider an ocean-based TC as such, regardless the position of the storm center. It is expected that by the end of 2018 the re-analysis of the TRMM-era rainfall data will be available from IMERG. Thus, a similar study to the one carried out here will benefit from the evaluation of almost 20 years of TC-rainfall.

An accurate description of the spatial (and temporal) TC-rainfall structure provides a path towards the development of improved TC-rainfall models. Such improved models potentially translate into our improved preparedness against

this type of natural hazards.

Acknowledgements

This material is based in part upon work supported by the National Science Foundation under Grants AGS-1262091 and AGS-1262099, and Award NA14OAR4830101 from the National Oceanic and Atmospheric Administration, U.S. Department of Commerce.

References

Alvey III, G. R., Zawislak, J., & Zipser, E. (2015). Precipitation properties observed during tropical cyclone intensity change. *Mon. Weather Rev.*, *143*, 4476–4492. doi:10.1175/MWR-D-15-0065.1.

Bender, M. A., Tuleya, R. E., & Kurihara, Y. (1985). A numerical study of the effect of a mountain range on a landfalling tropical cyclone. *Mon. Weather Rev.*, *113*, 567–583. doi:10.1175/1520-0493(1985)113<0567:ANSOTE>2.0.CO;2.

Czajkowski, J., Villarini, G., Montgomery, M., Michel-Kerjan, E., & Goska, R. (2017). Assessing current and future freshwater flood risk from north atlantic tropical cyclones via insurance claims. *Scientific Reports*, *7*. doi:10.1038/srep41609.

Elsberry, R. L. (2002). Predicting hurricane landfall precipitation: Optimistic and pessimistic views from the symposium on precipitation extremes. *Bull. Amer. Meteor. Soc.*, *83*, 1333–1339. doi:10.1175/1520-0477(2002)083<1333:PHLPOA>2.3.CO;2.

Emanuel, K. (2005). *Divine Wind - The History and Science of Hurricanes*. New York, USA: Oxford University Press.

Holland, G. (2008). A revised hurricane pressure-wind model. *Mon. Weather Rev.*, *136*, 3432–3445. doi:10.1175/2008MWR2395.1.

Hou, A. Y., Kakar, R. K., Neeck, S., Azarbarzin, A. A., Kummerow, C. D., Kojima, M., Oki, R., Nakamura, K., & Iguchi, T. (2014). The Global Precipitation Measurement mission. *Bull Amer Meteor Soc*, *95*, 701–722. doi:10.1175/BAMS-D-13-00164.1.

Huffman, G. J., Bolvin, D. T., Braithwaite, D., Hsu, K., Joyce, R., Kidd, C., Nelkin, E. J., Sorooshian, S., Tan, J., & Xie, P. (2017a). NASA Global Precipitation Measurement Integrated Multi-satellitE Retrievals for GPM (IMERG). Algorithm Theoretical Basis Document, version 4.6. NASA [online]. Mar 2017, 32 pp., https://pmm.nasa.gov/sites/default/files/document_files/IMERG_ATBD_V4.6.pdf, (accessed July 3, 2017).

Huffman, G. J., Bolvin, D. T., & Nelkin, E. J. (2017b). Integrated Multi-satellitE Retrievals for GPM (IMERG) Technical Documentation. NASA [online]. Mar 2017, 54 pp., https://pmm.nasa.gov/sites/default/files/document_files/IMERG_technical_doc_3_22_17.pdf, (accessed July 3, 2017).

Huffman, G. J., Bolvin, D. T., Nelkin, E. J., & Stocker, E. F. (2017c). V04 IMERG Final Run release notes. NASA Tech. Doc. NASA [online]. Mar 2017, 2 pp., https://pmm.nasa.gov/sites/default/files/document_files/IMERG_FinalRun_V04_release_notes-1.pdf, (accessed July 3, 2017).

Huffman, G. J., Bolvin, D. T., Nelkin, E. J., Wolff, D. B., Adler, R. F., Gu, G., Hong, Y., Bowman, K. P., & Stocker, E. F. (2007). The TRMM Multi-satellite Precipitation Analysis (TMPA): Quasi-global, multiyear, combined-sensor precipitation estimates at fine scales. *J. Hydrometeorol.*, *8*, 38–55. doi:10.1175/JHM560.1.

Impact Forecasting (2017). 2016 Annual global climate and catastrophe report. Aon Benfield [online]. Jan 2017, 75

pp., http://thoughtleadership.aonbenfield.com/Documents/20170117-ab-if-annual-climate-catastrophe-report.pdf, (accessed Jul 12, 2017).

Jiang, H., Halverson, J. B., Simpson, J., & Zipser, E. J. (2008a). Hurricane "rainfall potential" derived from satellite observations aids overland rainfall prediction. *Journal of Applied Meteorology and Climatology*, *47*, 944–959. doi:10.1175/2007JAMC1619.1.

Jiang, H., Halverson, J. B., & Zipser, E. J. (2008b). Influence of environmental moisture on TRMM-derived tropical cyclone precipitation over land and ocean. *Geophys. Res. Lett.*, *35*, n/a–n/a. doi:10.1029/2008GL034658. L17806.

Joyce, R. J., Janowiak, J. E., Arkin, P. A., & Xie, P. (2004). CMORPH: A method that produces global precipitation estimates from passive microwave and infrared data at high spatial and temporal resolution. *J Hydrometeor*, *5*, 487–503. doi:10.1175/1525-7541(2004)005<0487:CAMTPG>2.0.CO;2.

Kepert, J. D. (2010). Tropical cyclone structure and dynamics. In J. C. L. Chan, & J. D. Kepert (Eds.), *Global Perspectives on Tropical Cyclones: From Science to Mitigation* chapter 1. (pp. 3–53). Singapore: World Scientific Publishing Company. ISBN-13 978-981-4293-47-1, 444 pp.

Khouakhi, A., Villarini, G., & Vecchi, G. A. (2017). Contribution of tropical cyclones to rainfall at the global scale. *J. Climate*, *30*, 359–372. doi:10.1175/JCLI-D-16-0298.1.

Knapp, K. R., Kruk, M. C., Levinson, D. H., Diamond, H. J., & Neumann, C. J. (2010). The International Best Track Archive for Climate Stewardship (IBTrACS). *Bull. Amer. Meteor. Soc.*, *91*, 363–376. doi:10.1175/2009BAMS2755.1.

Langousis, A., & Veneziano, D. (2009). Theoretical model of rainfall in trop-

ical cyclones for the assessment of long-term risk. *Journal of Geophysical Research: Atmospheres*, *114*, n/a–n/a. doi:10.1029/2008JD010080. D02106.

Lin, Y., Zhao, M., & Zhang, M. (2015). Tropical cyclone rainfall area controlled by relative sea surface temperature. *Nat. Commun.*, *6*, 6591. doi:10.1038/ncomms7591.

Lonfat, M., Jr., F. D. M., & Chen, S. S. (2004). Precipitation distribution in tropical cyclones using the tropical rainfall measuring mission (TRMM) microwave imager: A global perspective. *Mon. Weather Rev.*, *132*, 1645–1660. doi:10.1175/1520-0493(2004)132<1645:PDITCU>2.0.CO;2.

Lonfat, M., Rogers, R., Marchok, T., & Jr., F. D. M. (2007). A parametric model for predicting hurricane rainfall. *Mon. Weather Rev.*, *135*, 3086–3097. doi:10.1175/MWR3433.1.

Luitel, B., Villarini, G., & Vecchi, G. A. (2016). Verification of the skill of numerical weather prediction models in forecasting rainfall from U.S. landfalling tropical cyclones. *J. Hydrol.*, . doi:10.1016/j.jhydrol.2016.09.019.

Marchok, T., Rogers, R., & Tuleya, R. (2007). Validation schemes for tropical cyclone quantitative precipitation forecasts: Evaluation of operational models for u.s. landfalling cases. *Wea. Forecasting*, *22*, 726–746. doi:10.1175/WAF1024.1.

Prat, O. P., & Nelson, B. R. (2013). Mapping the world's tropical cyclone rainfall contribution over land using the TRMM Multi-satellite Precipitation Analysis. *Water Resour. Res.*, *49*, 7236–7254. doi:10.1002/wrcr.20527.

Prat, O. P., & Nelson, B. R. (2016). On the link between tropical cyclones and daily rainfall extremes derived from global satellite observations. *J. Climate*, *29*, 6127–6135. doi:10.1175/JCLI-D-16-0289.1.

Rappaport, E. N. (2000). Loss of life in the united states associated with recent atlantic tropical cyclones. *Bull. Amer. Meteor. Soc.*, *81*, 2065–2073. doi:10.1175/1520-0477(2000)081<2065:LOLITU>2.3.CO;2.

Rappaport, E. N. (2014). Fatalities in the united states from atlantic tropical cyclones: New data and interpretation. *Bull. Amer. Meteor. Soc.*, *95*, 341–346. doi:10.1175/BAMS-D-12-00074.1.

Rios Gaona, M. F., Overeem, A., Leijnse, H., & Uijlenhoet, R. (2016). First-year evaluation of GPM rainfall over the Netherlands: IMERG Day 1 Final Run (V03D). *J Hydrometeor*, *17*, 2799–2814. doi:10.1175/JHM-D-16-0087.1.

Schneider, U., Becker, A., Finger, P., Meyer-Christoffer, A., Rudolf, B., & Ziese, M. (2015a). GPCC Full Data Reanalysis Version 7.0 at 0.5°: Monthly land-surface precipitation from rain-gauges built on GTS-based and historic data. doi:10.5676/DWD_GPCC/FD_M_V7_050.

Schneider, U., Becker, A., Finger, P., Meyer-Christoffer, A., & Ziese, M. (2015b). GPCC Monitoring Product: Near real-time monthly land-surface precipitation from rain-gauges based on SYNOP and CLIMAT data. doi:10.5676/DWD_GPCC/MP_M_V5_100.

Simpson, R. H. (1974). The hurricane disaster-potential scale. *Weatherwise*, *27*, 169–186. doi:10.1080/00431672.1974.9931702.

Stöckli, R., Vermote, E., Saleous, N., Simmon, R., & Herring, D. (2006). True color earth data set includes seasonal dynamics. *EOS, Transactions American Geophysical Union*, *87*, 49–55. doi:10.1029/2006EO050002.

Tuleya, R. E., DeMaria, M., & Kuligowski, R. J. (2007). Evaluation of gfdl and simple statistical model rainfall forecasts for u.s. landfalling tropical storms. *Weather Forecasting*, *22*, 56–70. doi:10.1175/WAF972.1.

Tustison, B., Harris, D., & Foufoula-Georgiou, E. (2001). Scale issues in verification of precipitation forecasts. *J. Geophys Res-Atmos*, *106*, 11775–11784. doi:10.1029/2001JD900066.

Villarini, G., Smith, J. A., Baeck, M. L., Marchok, T., & Vecchi, G. A. (2011). Characterization of rainfall distribution and flooding associated with

u.s. landfalling tropical cyclones: Analyses of hurricanes frances, ivan, and jeanne (2004). *Journal of Geophysical Research: Atmospheres*, *116*, n/a–n/a. doi:10.1029/2011JD016175. D23116.

Wang, Y., & Wu, C.-C. (2004). Current understanding of tropical cyclone structure and intensity changes – a review. *Meteorol. Atmos. Phys.*, *87*, 257–278. doi:10.1007/s00703-003-0055-6.

Wu, C.-C., Chou, K.-H., Cheng, H.-J., & Wang, Y. (2003). Eyewall contraction, breakdown and reformation in a landfalling typhoon. *Geophys. Res. Lett.*, *30*, n/a–n/a. doi:10.1029/2003GL017653. 1887.

Yu, Z., Wang, Y., Xu, H., Davidson, N., Chen, Y., Chen, Y., & Yu, H. (2017). On the relationship between intensity and rainfall distribution in tropical cyclones making landfall over china. *Journal of Applied Meteorology and Climatology*, *56*, 2883–2901. doi:10.1175/JAMC-D-16-0334.1.